NASA TECHNICAL MEMORANDUM

UB
NASA TM X-1196



# COMPARISON OF FREE-FLIGHT AND WIND-TUNNEL DATA FOR APOLLO LAUNCH ESCAPE VEHICLE AT MACH NUMBERS 0.7 AND 1.2

*by Robert L. Kruse and Barbara J. Short*

*Ames Research Center*
*Moffett Field, Calif.*

NATIONAL AERONAUTICS AND SPACE ADMINISTRATION • WASHINGTON, D. C. • JANUARY 1966

CONFIDENTIAL

[redacted]

NASA TM X-1196

# COMPARISON OF FREE-FLIGHT AND WIND-TUNNEL DATA FOR APOLLO LAUNCH ESCAPE VEHICLE AT MACH NUMBERS 0.7 AND 1.2

By Robert L. Kruse and Barbara J. Short

Ames Research Center
Moffett Field, Calif.

[redacted]

[redacted]

[redacted]

[redacted]

"Available to U.S. Government Agencies and U. S. Government Contractors Only"

NATIONAL AERONAUTICS AND SPACE ADMINISTRATION

[redacted]

# COMPARISON OF FREE-FLIGHT AND WIND-TUNNEL DATA FOR APOLLO LAUNCH ESCAPE VEHICLE AT MACH NUMBERS 0.7 AND 1.2*

By Robert L. Kruse and Barbara J. Short
Ames Research Center

## SUMMARY

An investigation was conducted with models of the Apollo Launch Escape Vehicle to determine the static- and dynamic-stability characteristics and drag. The static-stability and drag coefficients were obtained from low-amplitude oscillatory motions of the models and they compared reasonably well with wind-tunnel data. The dynamic stability appeared to be a function of the maximum angle of oscillation and Mach number.

## INTRODUCTION

In the event of a mission abort during the launching of the Project Apollo spacecraft, the escape rocket will separate the command module from the booster. The escape rocket, escape tower, and command module comprise the Launch Escape Vehicle (L.E.V.). Following burnout of the escape rocket during the abort maneuver, the L.E.V. will coast for a short period of time before the tower and rocket separate from the command module. Free-flight tests were conducted on models of the L.E.V. to determine the stability characteristics and drag during the coasting phase of the abort maneuver. The tests were conducted in the Ames Pressurized Ballistic Range at nominal Mach numbers 0.7 and 1.2, with corresponding Reynolds numbers of $0.8\times10^6$ and $1.4\times10^6$ based on free-stream conditions and model diameter. The higher Mach number and Reynolds number conditions roughly correspond to the abort conditions at 60,000 feet altitude.

## SYMBOLS

| | |
|---|---|
| $A$ | frontal area |
| $C_A$ | axial force coefficient, $\frac{\text{axial force}}{qA}$, dimensionless |
| $C_D$ | drag coefficient, $\frac{\text{drag}}{qA}$, dimensionless |
| $C_L$ | lift coefficient, $\frac{\text{lift}}{qA}$, dimensionless |

| | |
|---|---|
| $C_{L_\sigma}$ | lift-curve slope, $\left(\frac{\partial C_L}{\partial \sigma}\right)_{\sigma \to 0}$, per radian |
| $C_m$ | pitching-moment coefficient, $\frac{\text{pitching moment}}{qAd}$, dimensionless |
| $C_{m_\sigma}$ | rate of change of $C_m$ with $\sigma$, $\left(\frac{\partial C_m}{\partial \sigma}\right)_{\sigma_{trim}}$, per radian |
| $(C_{m_q} + C_{m_{\dot{\sigma}}})$ | damping-in-pitch derivative, $\frac{\partial C_m}{\partial(\dot{\theta}d/v)} + \frac{\partial C_m}{\partial(\dot{\sigma}d/v)}$, dimensionless |
| $C_N$ | normal force coefficient, $\frac{\text{normal force}}{qA}$, dimensionless |
| d | maximum diameter of model, ft |
| $I_x$ | moment of inertia about a longitudinal axis through the center of gravity, slug-ft$^2$ |
| $I_y$ | moment of inertia about a transverse axis through the center of gravity and perpendicular to the plane of mass symmetry, slug-ft$^2$ |
| $K_{1,2,3}$ | constants in equation (1), deg |
| m | mass of model, slugs |
| p | roll parameter, $\frac{\text{roll rate}}{\text{velocity}}$, radians/ft |
| q | free-stream dynamic pressure, lb/ft$^2$ |
| R | Reynolds number based on maximum diameter and free-stream conditions, dimensionless |
| $r_g$ | radius of gyration about a transverse axis through the center of gravity and perpendicular to the plane of mass symmetry, ft |
| v | velocity along flight path, ft/sec |
| x | distance along flight path, ft |
| $X_{cg}$ | axial distance from center of heat shield to center-of-gravity position, ft |
| $Z_{cg}$ | transverse distance from model center line to center-of-gravity position, ft |
| $\alpha$ | angle of attack (in the vertical plane), deg |
| $\beta$ | angle of sideslip (in the horizontal plane), deg |
| $\eta_{1,2}$ | damping exponents in equation (1), ft$^{-1}$ |

$\theta$ angle between body axis and horizontal, deg

$\lambda$ wave length of pitching oscillation, ft/cycle

$\xi$ dynamic-stability parameter, $C_D - C_{L_\sigma} + (C_{m_q} + C_{m_{\dot{\sigma}}}) \left(\frac{d}{r_g}\right)^2$

$\rho$ free-stream air density, slugs/ft$^3$

$\sigma$ resultant angle of attack, $\tan^{-1} \sqrt{\tan^2 \alpha + \tan^2 \beta}$, deg

$\sigma_m$ maximum resultant angle of attack, deg

$\sigma_{rms}$ root-mean-square angle of attack, $\sqrt{\frac{\int_o^x \sigma^2 \, dx}{x}}$, deg

$\omega$ frequency of pitching oscillation, radians/sec

$\omega_{1,2}$ rates of rotation of vectors which describe the model pitching motion, radians/ft

$\frac{\omega d}{2v}$ reduced frequency parameter, dimensionless

## MODELS AND TEST CONDITIONS

A sketch of the model used in this investigation is shown in figure 1. For these scaled models, the complex escape-tower structure of the full-scale vehicle was simplified to have four members. For the first model launched, the tower was further simplified to reduce machining time; it consisted of a single member 0.128 inch in diameter (see fig. 2(a)). A comparison of figures 2(a) and (b) shows no obvious differences in the flow characteristics of the two models with different tower simplifications and there was no apparent effect on the aerodynamic characteristics. However, with the four-member simplification the roll rate could be estimated from the spacing between the four members on successive shadowgraphs. This was found to be helpful in analyzing the motions, and the four-member simplification was used in all subsequent tests.

The models were machined from 7075-T6 aluminum alloy and had a maximum diameter of 2 inches. They were ballasted with a tungsten alloy to give the desired center-of-gravity location, which corresponds to burnout conditions of the escape rocket. The four-member tower was made of 1/16-inch-diameter music wire.

The investigation was conducted in the Ames Pressurized Ballistic Range. Time-distance and attitude histories were recorded at 24 spark-shadowgraph stations along its 203-foot length. The models were gun launched into atmospheric air and tested at two nominal Mach numbers, 0.7 and 1.2. The corresponding Reynolds numbers were $0.8 \times 10^6$ and $1.4 \times 10^6$ based on free-stream conditions and model diameter. Because of the asymmetry of the model, it trimmed at an angle

of attack of about $2^{\circ}$ and lifted or swerved out of the instrumented region of the range after 120 to 160 feet of flight. A model and sabot are shown in figure 3.

## DATA REDUCTION

The stability data were obtained from analyses of the pitching and yawing motions of each flight. The following equation was fitted to measured values of $\alpha$ and $\beta$ by a least-squares fit

$$\beta + i\alpha = K_1 e^{(\eta_1 + i\omega_1)x} + K_2 e^{(\eta_2 - i\omega_2)x} + K_3 e^{ipx} \tag{1}$$

Equation (1) is the solution of the linear differential equation of motion as given in reference 1. In the development of the equation a linear force and moment system was assumed.

The static-stability parameter, $C_{m_\sigma}$, was computed from the wave length of oscillation by means of the relation

$$C_{m_\sigma} = \frac{-4\pi^2 d}{\lambda^2 \left(\frac{\rho A}{2m}\right)\left(\frac{d}{r_g}\right)^2}$$

where

$$\lambda = \frac{2\pi}{\sqrt{\omega_1 \omega_2}}$$

The dynamic-stability parameter, $\xi$, was determined from the constants $\eta_1$ and $\eta_2$ by means of the relation

$$\eta_1 + \eta_2 = \frac{\rho A}{2m} \xi$$

where

$$\xi = C_D - C_{L_\sigma} + (C_{m_q} + C_{m_{\dot{\sigma}}})\left(\frac{d}{r_g}\right)^2$$

The roll parameter, p, is related to the constants $\omega_1$ and $\omega_2$ by the relation

$$p = \frac{I_y}{I_x} (\omega_1 - \omega_2) \tag{2}$$

The data-reduction program was unable, in most cases, to give an acceptable fit of equation (1) to all the values of $\alpha$ and $\beta$ of a complete flight.

This was due to the high $I_y/I_x$ ratio of the models which caused p (see eq. (2)) to be sufficiently large that it had a significant influence on the fit of equation (1) to the data. Consequently, in order to get the best fit of equation (1) to the values of $\alpha$ and $\beta$ of a flight, it was necessary, in most cases, to divide each flight approximately in half and analyze each half separately.

Free-flight motions of the L.E.V. models in the $\alpha$-$\beta$ plane are shown in figure 4. The motions are typical of an asymmetric rolling body since they are not symmetric about the origin nor are the ellipses of uniform eccentricity. The numbered data points correspond to the stations at which the model had that $\alpha$ and $\beta$. The stations are not equally spaced and the nominal station distances are given in table I. The reading accuracy of these angles is approximately $\pm 0.10^{\circ}$. The curves are the best fit of equation (1) to the data points. Because of the questionable fit of equation (1) to the data points, the reliability of the stability data reduced from the tests was investigated. Test 647, figure 4(a), was chosen for the investigation because the fit of equation (1) had the greatest least-squares error. Also presented in figure 4(a) is a dashed curve hand faired through the data points. Plots of $\alpha$ and $\beta$ vs x were used as an aid in fairing this curve. From this curve, a resultant angle-of-attack plot was constructed from which wave lengths were taken. For stations 1 through 13, a wave length of 57 feet was determined from the faired curve as compared to 55.6 feet found from the fit of equation (1) resulting in a difference in $C_{m_\sigma}$ of 4 percent. For stations 11 through 21, a wave length of 61 feet was determined from the faired curve as compared to 62.1 feet from the fit of equation (1) resulting in a difference in $C_{m_\sigma}$ of 3 percent. It is seen that while the fitted curve appears to have a rather large error in the fit, there is not a great difference between the values of $C_{m_\sigma}$ determined by the two methods. A difference in $\xi$ could not be determined in a similar manner; however, a qualitative comparison can be made by observing the peaks of the faired and fitted curves. It can be seen that the peaks of the faired curve increase in amplitude as do those of the fitted curve.

The drag coefficient, $C_D$, was determined from the deceleration of the model by the procedure described in reference 2.

## RESULTS AND DISCUSSION

The physical characteristics of the models are given in table II. Data from four flights at $M \approx 0.7$ and two at $M \approx 1.2$ are given in table III. In the column labeled "Included stations" the first group of stations for each test number indicates the length of flight before the model swerved out of the instrumented region of the range. From this group of stations, drag data are obtained. Also listed in this column are partial tests from which stability data are obtained. Test 654, however, has all the data in one entry and test 655, which has no reduced data, will be discussed separately.

The wind-tunnel data from Ames Unitary Plan Wind Tunnel and AEDC Von Kármán Facility Tunnel A, with which the data of this investigation are compared, are given in table IV.

## Static Stability

The static-stability results are presented in figure 5. In figure 5(a) the static-stability parameter, $C_{m_\sigma}$, is plotted as a function of $\sigma_m$. The data points from the subsonic tests which were at nearly the same Mach numbers are connected by dashed lines showing the influence of amplitude on static stability. The data points from the supersonic tests have nearly the same $\sigma_m$, $3^\circ$ to $3.5^\circ$. The apparent scatter can be largely attributed to the variation in Mach number as seen in figure 5(b), where $C_{m_\sigma}$ is plotted versus Mach number. Also shown in figure 5(b) are the upper and lower envelopes of slopes taken from figure 6 in which the wind-tunnel data are transferred to the moment center of the models of the present investigation. Since the wind-tunnel data were furnished for only $5^\circ$ angle-of-attack intervals, the shape of the curve faired through the points is subject to some uncertainty, as is the static-stability parameter, $C_{m_\sigma}$, taken at the trim point ($\alpha \approx 1.5^\circ$). It is seen in figure 5(b) that the present results agree substantially with the wind-tunnel data.

The resultant angle-of-attack history for test 655, listed in table III with no reduced data, is shown in figure 7. It is speculated that during the sabot separation the model received an unusually large disturbance causing the model to exceed the limit of static stability, about $30^\circ$ as determined from wind-tunnel tests. The model then rotated to an angle of attack of about $300^\circ$ and reversed its rotation. From the limited amount of motion, it could not be determined whether the model would return to the nose-forward attitude, oscillate heat-shield forward, or tumble.

## Dynamic Stability

The dynamic-stability results are shown in figure 8. The parameter $\xi$ is presented as a function of $\sigma_m$ in figure 8(a). The fit of equation (1) to the data points is insensitive to small changes in the parameters $\eta_1$ and $\eta_2$ and, since $\xi$ is determined from these parameters, some scatter is expected. However, there appears to be a trend of decreasing stability with increasing maximum angle of oscillation. The influence of Mach number on the dynamic stability can be seen in figure 8(b). The trend of decreasing stability with increasing Mach number appears to have a discontinuity between the subsonic and supersonic Mach numbers; the data might also be interpreted as showing an overall increase in dynamic stability with Mach number. The effects of Mach number and amplitude of oscillation on $\xi$ could not be separated; however, it is possible that the results of the subsonic tests were more influenced by amplitude, while the supersonic tests were at nearly the same amplitude and thus more influenced by Mach number as was the case for the static-stability results. Figure 9, which is a crossplot of figures 5 and 8, shows the dynamic-stability parameter, $\xi$, as a variation of the pitching-moment-curve slope, $C_{m_\sigma}$. It can be seen that there is an increase in dynamic stability with an increase in static stability.

### Drag

The drag coefficient, $C_D$, was deduced from the data by the method described in reference 2 and is plotted as a function of average Mach number for each run in figure 10. Also shown for comparison are wind-tunnel values interpolated from figure 11 for the $\sigma_{rms}$ and Mach number of each run. The drag curves of figure 11 were calculated from the wind-tunnel axial- and normal-force data.

The agreement between free-flight and wind-tunnel drag data in figure 10 is generally quite good. The free-flight data, however, are consistently higher than the wind-tunnel data. The difference is possibly due to the lower Reynolds numbers of the free-flight tests. At Mach numbers 0.7 and 1.2 the Reynolds numbers of the wind-tunnel tests were $2.9 \times 10^6$ and $3.7 \times 10^6$, respectively, while the corresponding Reynolds numbers of the free-flight tests were $0.8 \times 10^6$ and $1.4 \times 10^6$. In addition, differences in base pressure could be a factor. Base-pressure corrections have not been applied to the wind-tunnel data, whereas true base pressure is implicit in the free-flight data.

## CONCLUDING REMARKS

Free-flight investigations have been made of models of the Apollo Launch Escape Vehicle at nominal Mach numbers 0.7 and 1.2 and the results have been compared with wind-tunnel data. The model was found to be statically stable nose forward up to the maximum angle tested, $7.6^\circ$, and the results were in substantial agreement with wind-tunnel data.

The dynamic stability appeared to decrease as the maximum angle of oscillation was increased, and to increase as the static stability was increased.

The drag was measured and found to compare reasonably well with wind-tunnel data.

Ames Research Center
National Aeronautics and Space Administration
Moffett Field, Calif., Sept. 28, 1965

## REFERENCES

1. Nicolaides, John D.: On the Free-Flight Motion of Missiles Having Slight Configurational Asymmetries. BRL Rep. 858, Aberdeen Proving Ground, Md., 1953.

2. Seiff, Alvin: A New Method for Computing Drag Coefficients From Ballistic Range Data. J. Aerospace Sci., vol. 25, no. 2, Feb. 1958, pp. 133-134.

TABLE I.- NOMINAL STATION DISTANCES

| Station | Distance, ft | Station | Distance, ft |
|---|---|---|---|
| 1 | 0 | 13 | 101.5 |
| 2 | 7 | 14 | 108.5 |
| 3 | 14 | 15 | 115.5 |
| 4 | 21 | 16 | 122.5 |
| 5 | 28 | 17 | 129.5 |
| 6 | 35 | 18 | 140 |
| 7 | 42 | 19 | 150.5 |
| 8 | 56 | 20 | 161 |
| 9 | 66.5 | 21 | 171.5 |
| 10 | 77 | 22 | 182 |
| 11 | 87.5 | 23 | 192.5 |
| 12 | 94.5 | 24 | 203 |

TABLE II.- PHYSICAL CHARACTERISTICS OF MODELS

| Run number | d, in. | Mass, slugs | $\frac{X_{cg}}{d}$ | $\frac{Z_{cg}}{d}$ | $\frac{l}{d}$ | $I_y \times 10^4$, slug-ft$^2$ | $I_x \times 10^5$, slug-ft$^2$ | $\left(\frac{d}{r_g}\right)^2$ |
|---|---|---|---|---|---|---|---|---|
| 647 | 1.998 | 0.00996 | 0.720 | 0.038 | 3.146 | 2.43 | 1.70 | 1.13 |
| 654 | 1.998 | .01000 | .712 | .037 | 3.152 | 2.34 | 1.70 | 1.18 |
| 655 | 2.003 | .01014 | .716 | .037 | 3.184 | 2.46 | 1.75 | 1.15 |
| 657 | 2.001 | .01011 | .710 | .035 | 3.146 | 2.38 | 1.75 | 1.18 |
| 666 | 1.999 | .01012 | .708 | .035 | 3.149 | 2.36 | 1.75 | 1.19 |
| 668 | 1.999 | .01012 | .709 | .036 | 3.149 | 2.38 | 1.74 | 1.18 |

TABLE III.- TEST CONDITIONS AND FINAL DATA

| Test number | Included stations | M | $R \times 10^{-6}$ | V, ft/sec | $\sigma_{rms}$, deg | $\sigma_m$, deg | $C_D$ | $C_{m_\sigma}$ | $\xi$ | $\frac{\omega d}{2v}$ |
|---|---|---|---|---|---|---|---|---|---|---|
| 647 | 1 - 21 | 0.72 | 0.81 | 817 | 3.5 | --- | 0.64 | --- | --- | --- |
| | 1 - 13 | .74 | .84 | 847 | --- | 5.92 | --- | -0.74 | 1.4 | 0.0094 |
| | 11 - 21 | .65 | .74 | 740 | --- | 6.88 | --- | -.60 | 3.0 | .0084 |
| 654 | 1 - 15 | 1.31 | 1.50 | 1480 | 2.3 | 3.54 | .88 | -.84 | -.4 | .0102 |
| 657 | 1 - 19 | 0.62 | 0.76 | 691 | 3.1 | --- | .63 | --- | --- | --- |
| | 1 - 9 | .66 | .80 | 736 | --- | 5.03 | --- | -.86 | 3.1 | .0106 |
| | 8 - 19 | .59 | .72 | 658 | --- | 5.05 | --- | -.82 | -1.8 | .0103 |
| 666 | 1 - 20 | .74 | .87 | 832 | 4.7 | --- | .65 | --- | --- | --- |
| | 1 - 10 | .78 | .92 | 880 | --- | 7.14 | --- | -.60 | 5.1 | .0087 |
| | 8 - 17 | .72 | .84 | 805 | --- | 7.60 | --- | -.60 | 2.2 | .0087 |
| 668 | 1 - 20 | 1.16 | 1.35 | 1303 | 2.1 | --- | .93 | --- | --- | --- |
| | 1 - 11 | 1.24 | 1.45 | 1400 | --- | 3.33 | --- | -.97 | -2.1 | .0110 |
| | 10 - 20 | 1.04 | 1.21 | 1168 | --- | 3.15 | --- | -1.19 | -5.1 | .0122 |
| 655 | 1 - 14 | 0.75 | 0.84 | 862 | --- | --- | --- | --- | --- | --- |

TABLE IV.- WIND-TUNNEL DATA

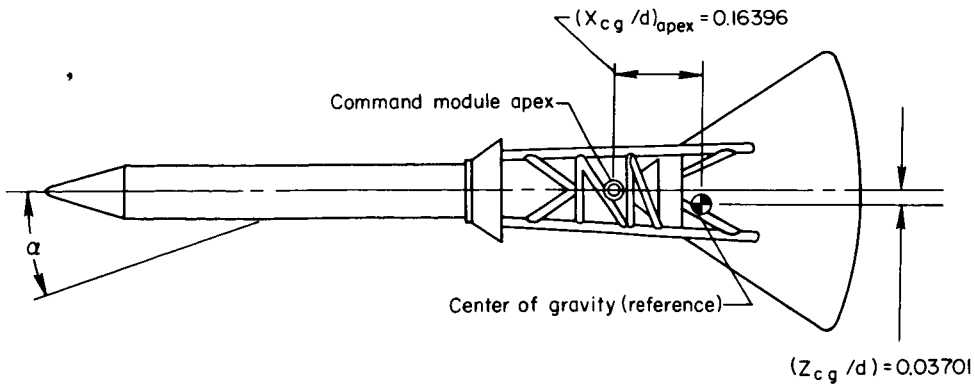


| Mach number | α | $C_A$ | $C_N$ | $C_{m_{cg}}$ | $C_{m_{apex}}$ |
|---|---|---|---|---|---|
| 0.50000 | 0 | 0.4540 | -0.0150 | 0.0093 | -0.0050 |
| | 5.00 | .5050 | .1550 | -.0459 | -.0900 |
| | 10.00 | .5300 | .2210 | -.0241 | -.0800 |
| | 15.00 | .4900 | .2800 | -.0250 | -.0890 |
| | 20.00 | .4560 | .3500 | -.0207 | -.0950 |
| 0.70000 | 0 | .5220 | -.0150 | .0319 | .0150 |
| | 5.00 | .6130 | .1700 | -.0344 | -.0850 |
| | 10.00 | .6050 | .2380 | -.0486 | -.1100 |
| | 15.00 | .5770 | .3000 | -.0535 | -.1240 |
| | 20.00 | .5370 | .3780 | -.0541 | -.1360 |
| 0.90000 | 0 | .6300 | -.0050 | .0305 | .0080 |
| | 5.00 | .7260 | .1850 | -.0478 | -.1050 |
| | 10.00 | .7520 | .2600 | -.0555 | -.1260 |
| | 15.00 | .7200 | .3250 | -.0591 | -.1390 |
| | 20.00 | .6700 | .4050 | -.0598 | -.1510 |
| 1.00000 | 0 | .8000 | 0 | .0336 | .0040 |
| | 5.00 | .9450 | .1780 | -.0368 | -.1010 |
| | 10.00 | .9650 | .2530 | -.0438 | -.1210 |
| | 15.00 | .8540 | .3120 | -.0482 | -.1310 |
| | 20.00 | .8500 | .3980 | -.0353 | -.1320 |
| 1.10000 | 0 | .9000 | .0050 | .0341 | 0 |
| | 5.00 | .9860 | .1700 | -.0336 | -.0980 |
| | 10.00 | .9870 | .2480 | -.0428 | -.1200 |
| | 15.00 | .9450 | .3050 | -.0380 | -.1230 |
| | 20.00 | .8920 | .3850 | -.0239 | -.1200 |
| 1.17000 | 0 | .8050 | .0020 | .0351 | .0050 |
| | 5.00 | .9060 | .1780 | -.0433 | -.1060 |
| | 10.00 | .9300 | .2680 | -.0576 | -.1360 |
| | 15.00 | .8950 | .3300 | -.0488 | -.1360 |
| | 20.00 | .8550 | .3970 | -.0283 | -.1250 |
| 1.27000 | 0 | .8040 | 0 | .0328 | .0030 |
| | 5.00 | .9000 | .1800 | -.0442 | -.1070 |
| | 10.00 | .9220 | .2810 | -.0698 | -.1500 |
| | 15.00 | .8980 | .3400 | -.0560 | -.1450 |
| | 20.00 | .8600 | .4240 | -.0306 | -.1320 |
| 1.48000 | 0 | .7540 | 0 | .0339 | .0060 |
| | 5.00 | .8400 | .1750 | -.0442 | -.1040 |
| | 10.00 | .9000 | .2900 | -.0851 | -.1660 |
| | 15.00 | .9290 | .3700 | -.0579 | -.1530 |
| | 20.00 | .9200 | .4650 | -.0147 | -.1250 |

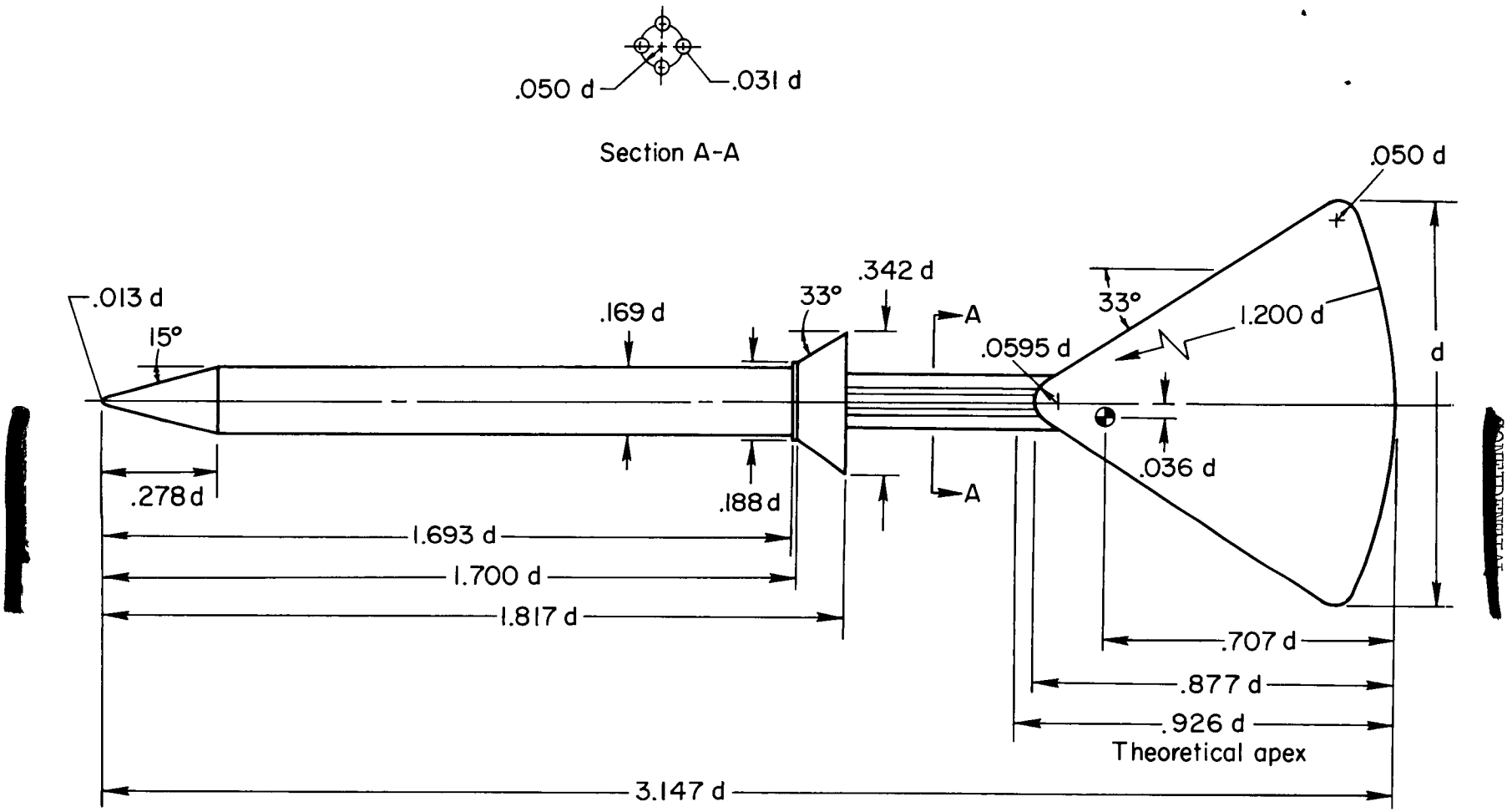


Figure 1.- Apollo Launch Escape Vehicle model.

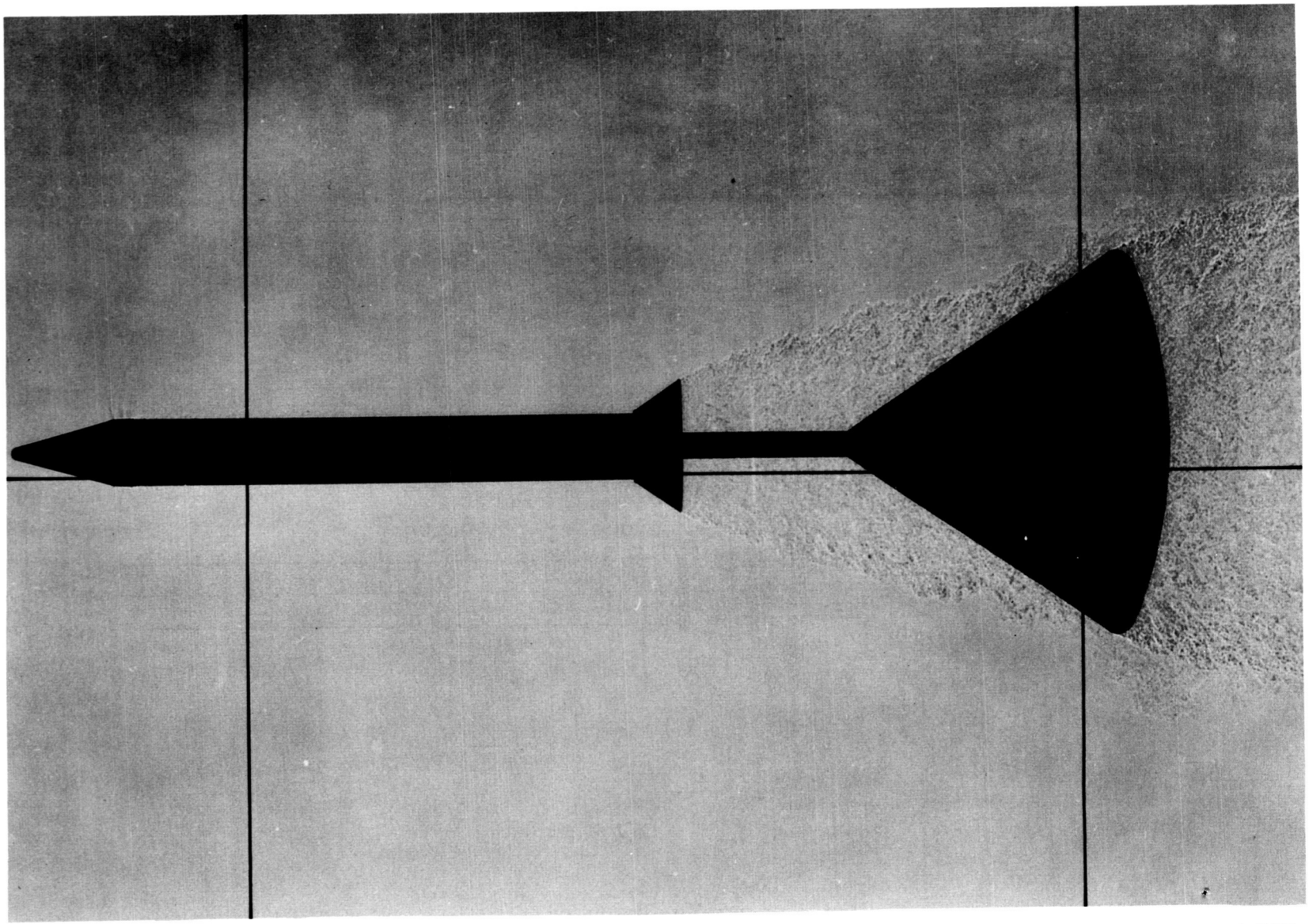

A-31200

(a) M = 0.78, R = $0.88 \times 10^6$, $\alpha = 0.2^\circ (\beta = 1.1^\circ)$

Figure 2.- Typical shadowgraphs of Launch Escape Vehicle model in flight.

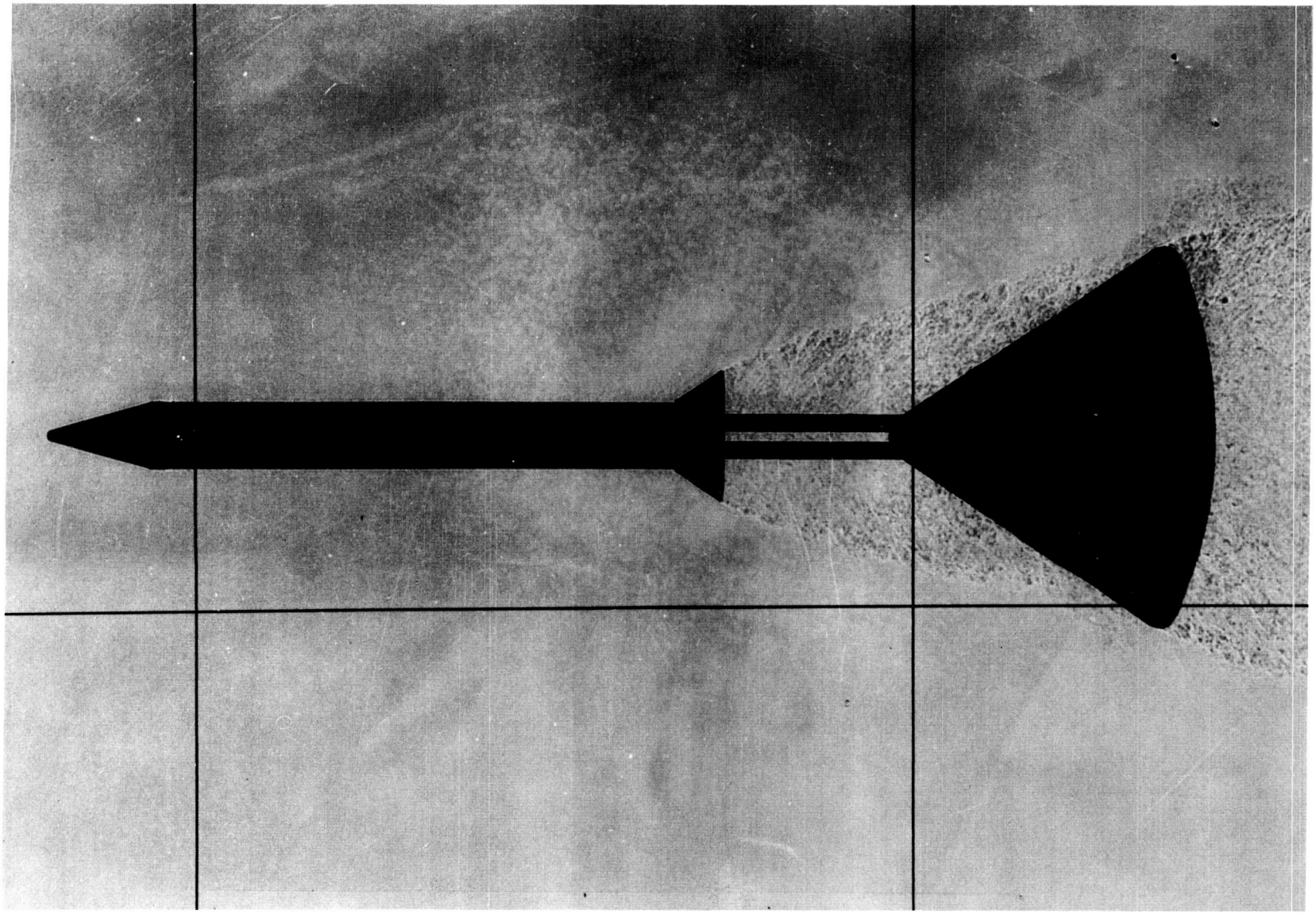

(b) $M = 0.72$, $R = 0.85 \times 10^6$, $\alpha = 0.32^\circ (\beta = -0.55^\circ)$

Figure 2.- Concluded.

Figure 3.- Apollo Launch Escape Vehicle model and sabot.

A-32139

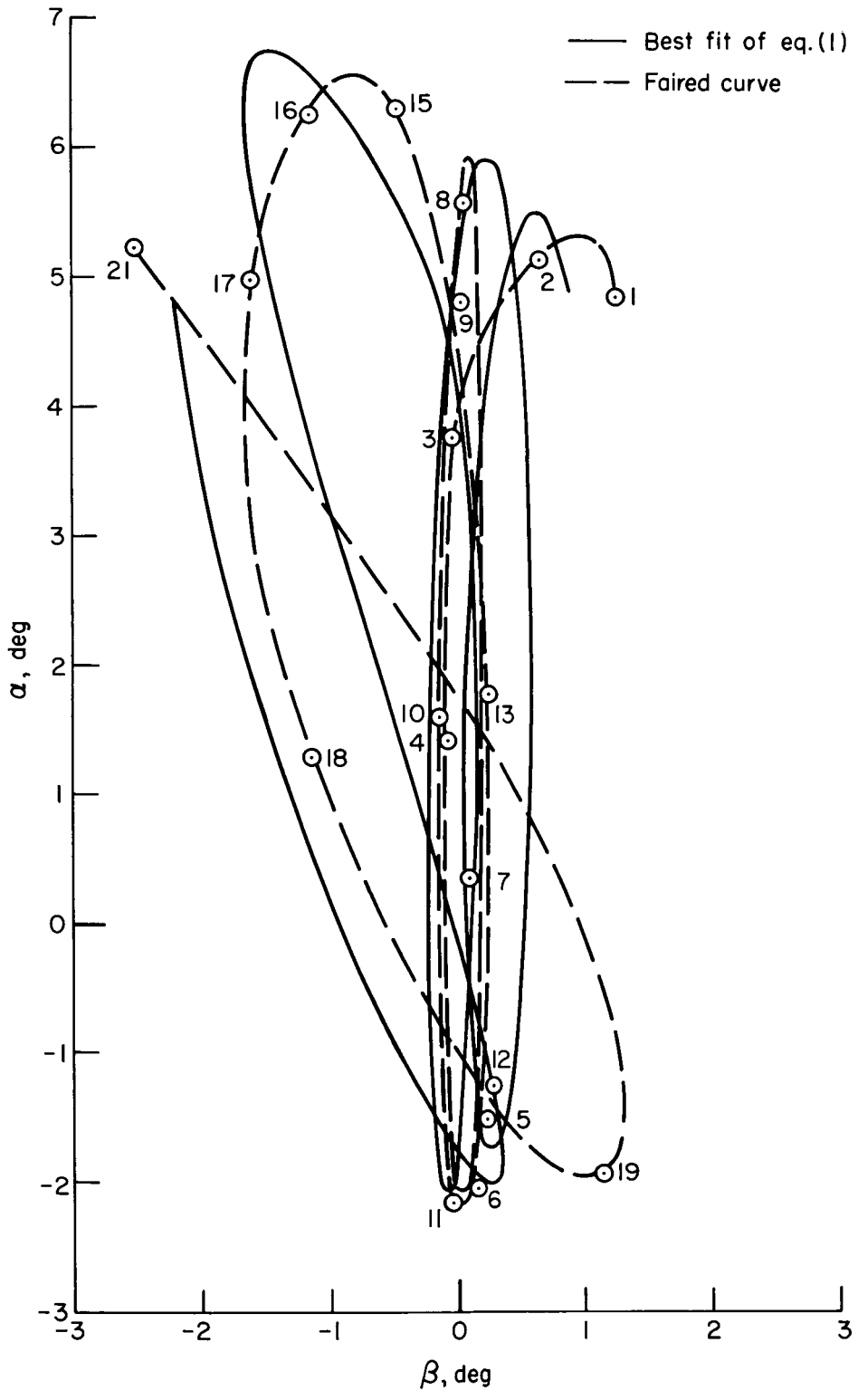


(a) Test 647, M = 0.72.

Figure 4.- Free-flight motions.

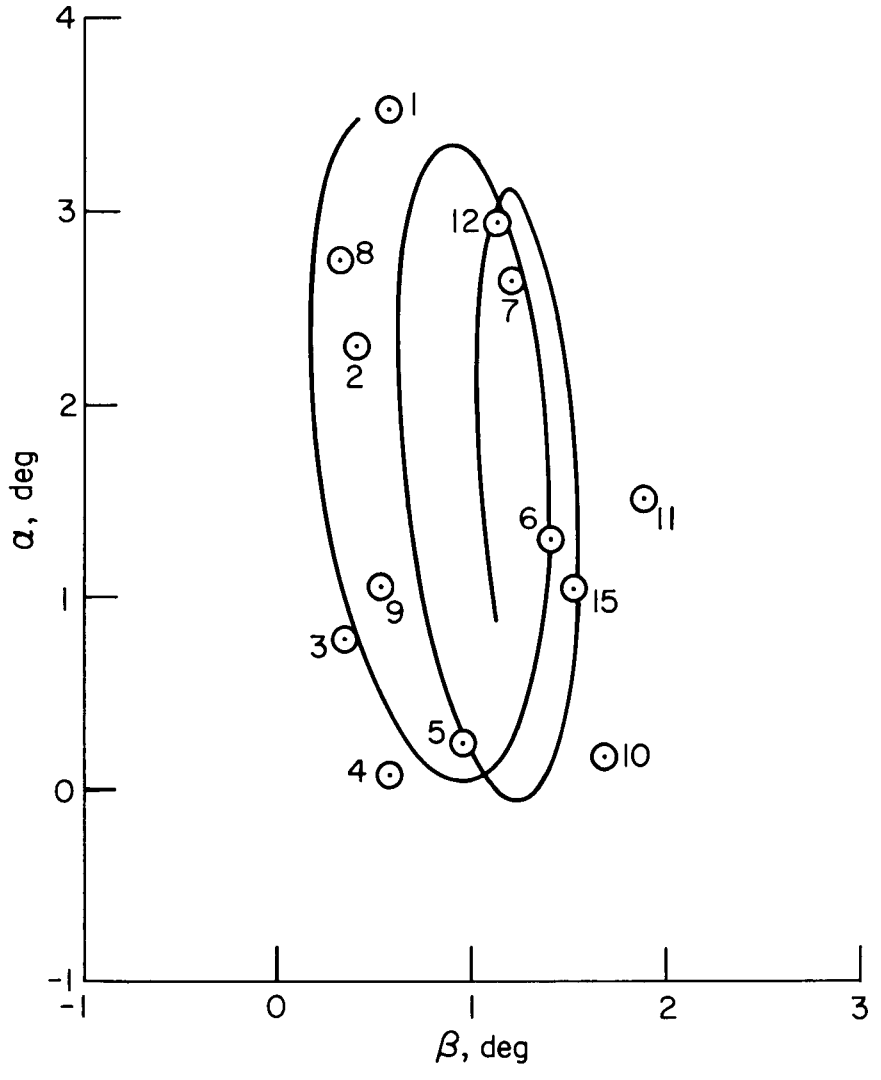


(b) Test 654, M = 1.31.

Figure 4.- Continued.

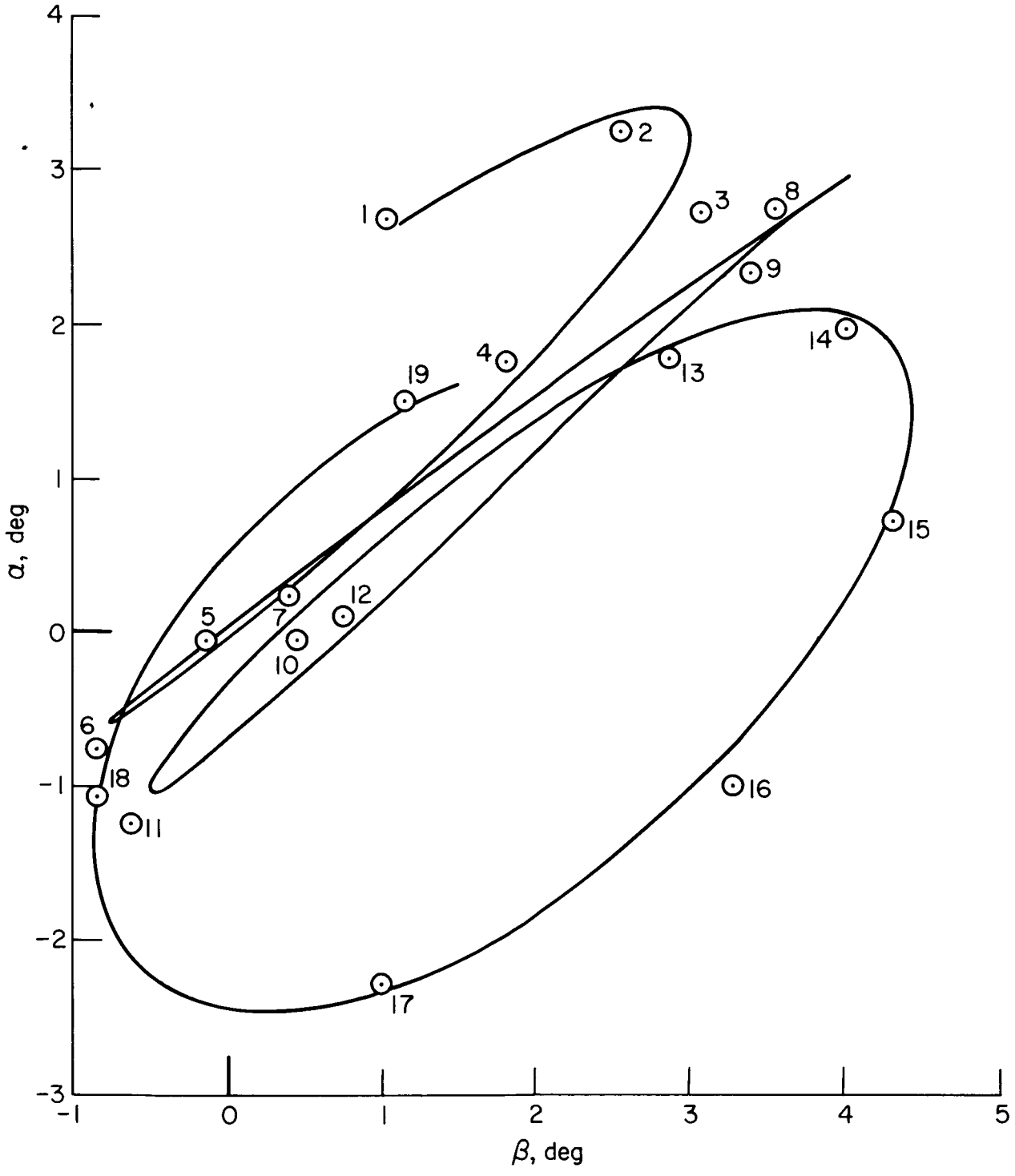


(c) Test 657, M = 0.62.

Figure 4.- Continued.

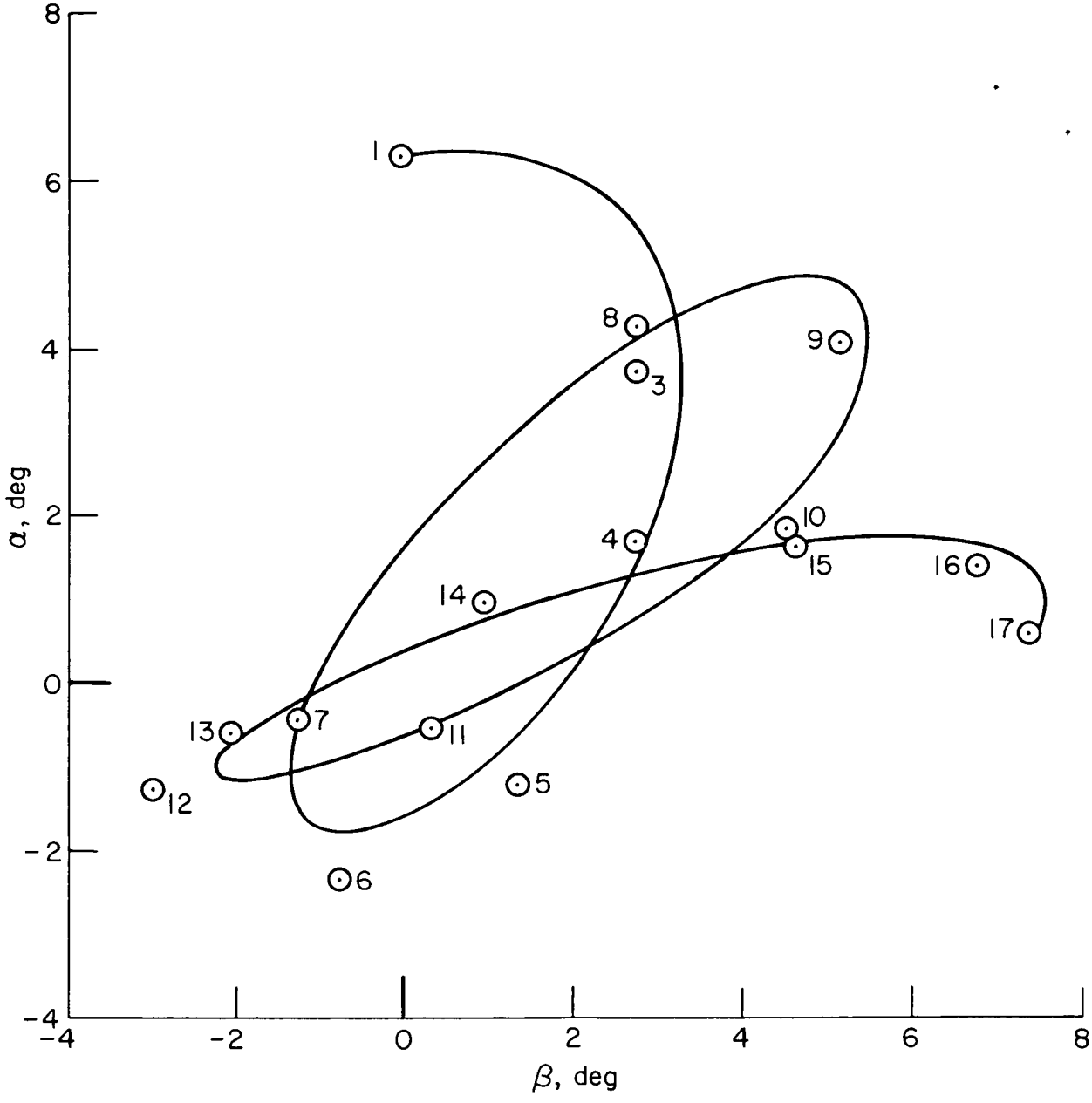


(d) Test 666, M = 0.74.

Figure 4.- Continued.

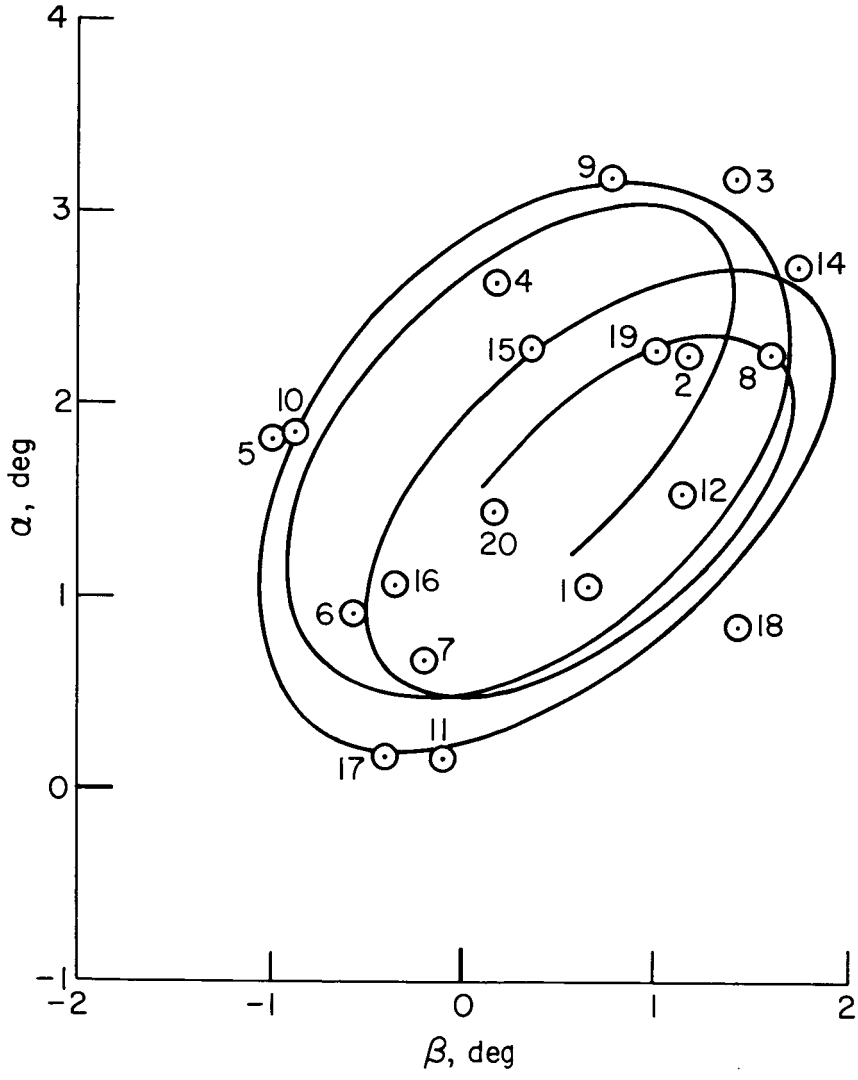


(e) Test 668, M = 1.16.

Figure 4.- Concluded.

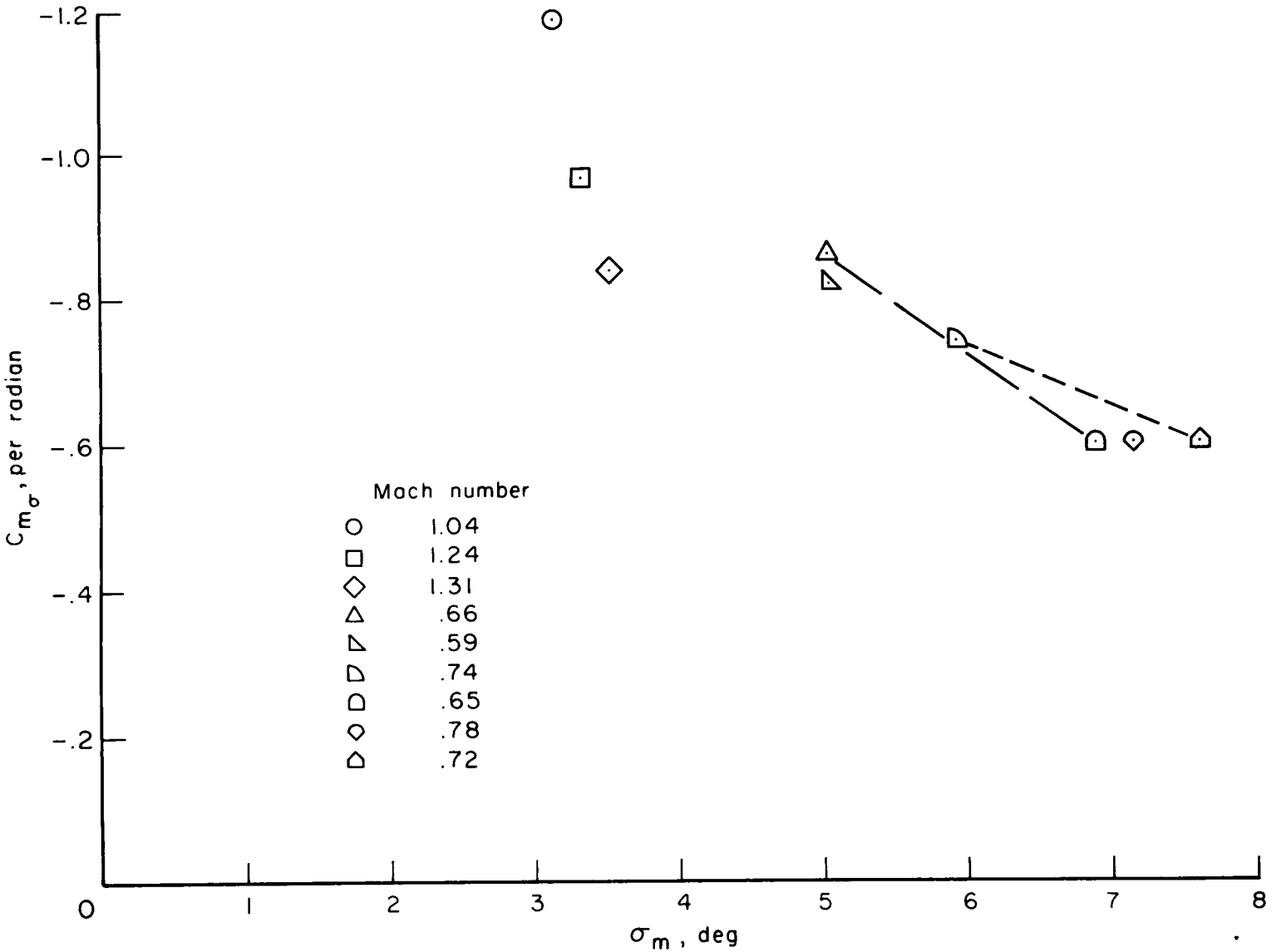


(a) Variation of static-stability parameter with $\sigma_m$.

Figure 5.- Static stability.

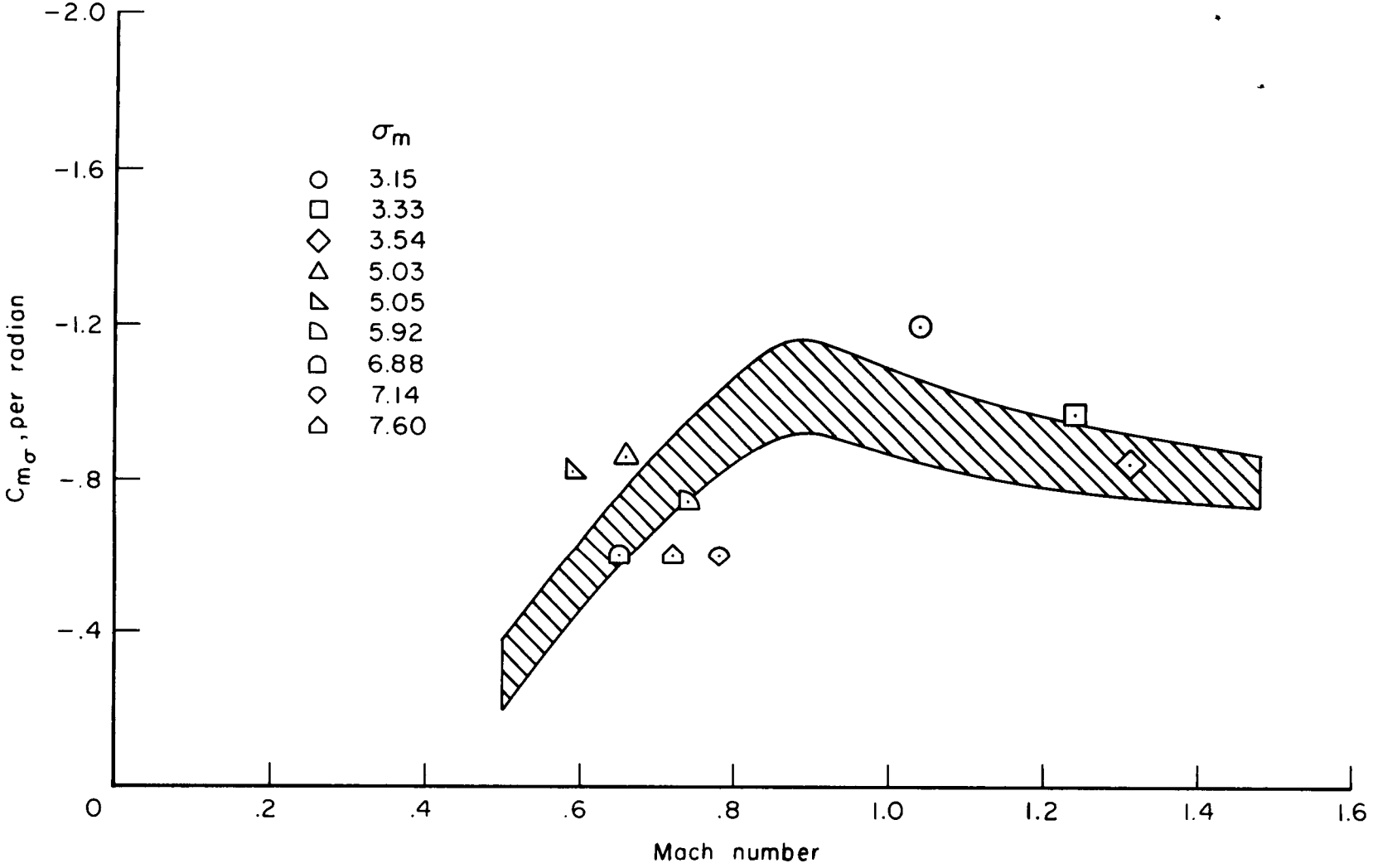


(b) Variation of static-stability parameter with Mach number.

Figure 5.- Concluded.

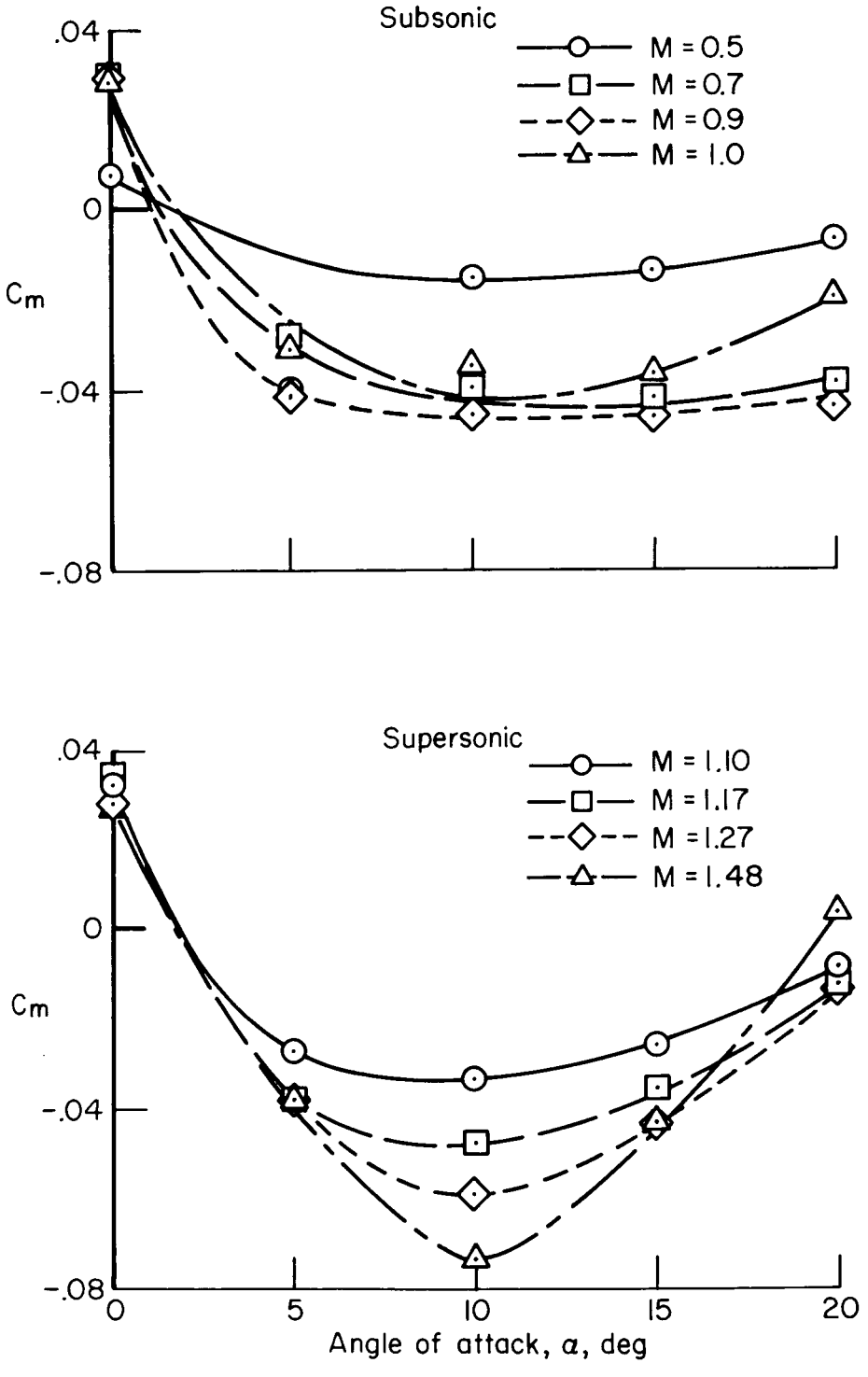


Figure 6.- Wind-tunnel data transferred to a moment center at $X_{cg}/d = 0.707$, $Z_{cg}/d = 0.036$.

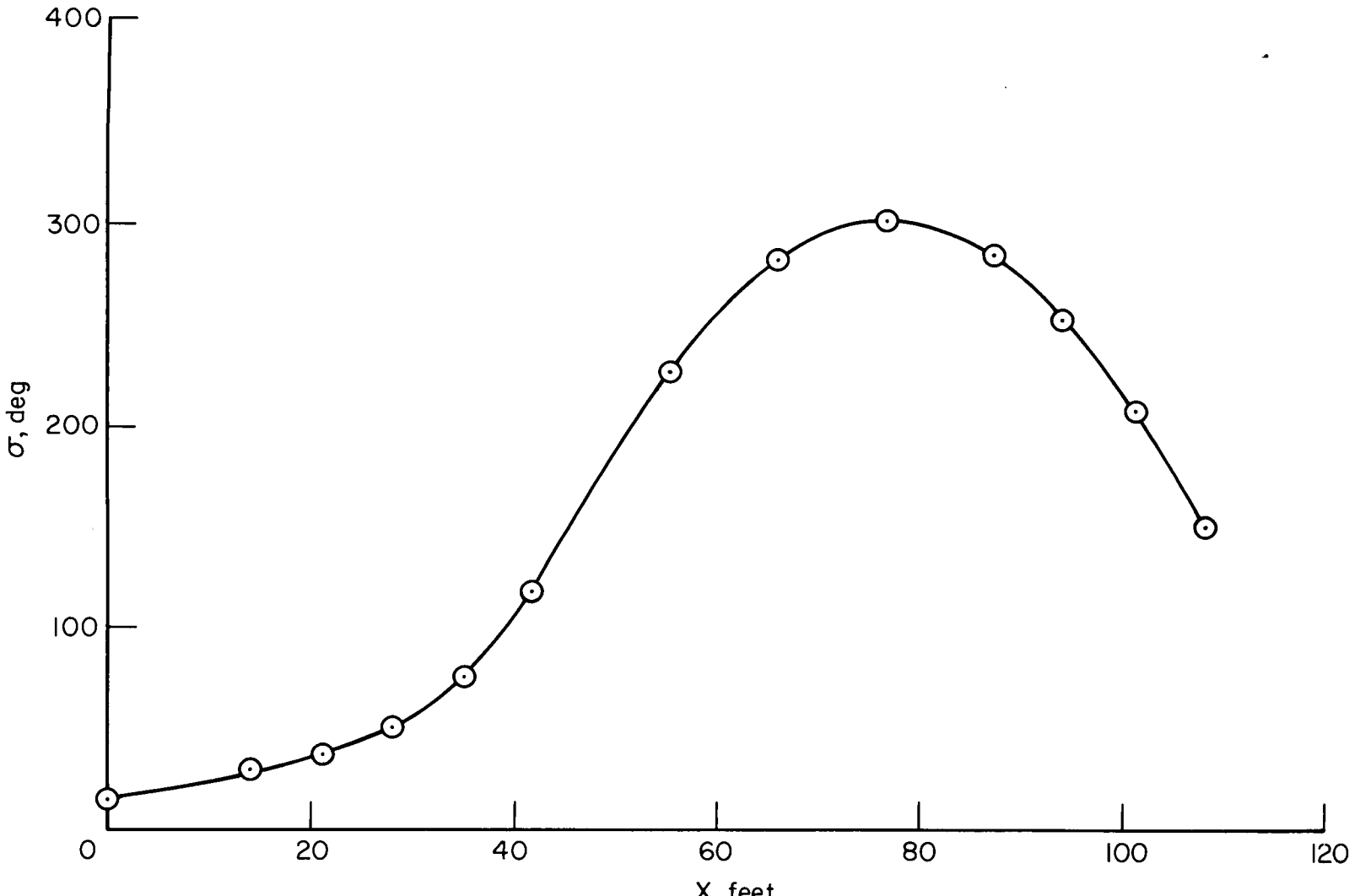


Figure 7.- Motion of model after large disturbance; test 655, M = 0.75.

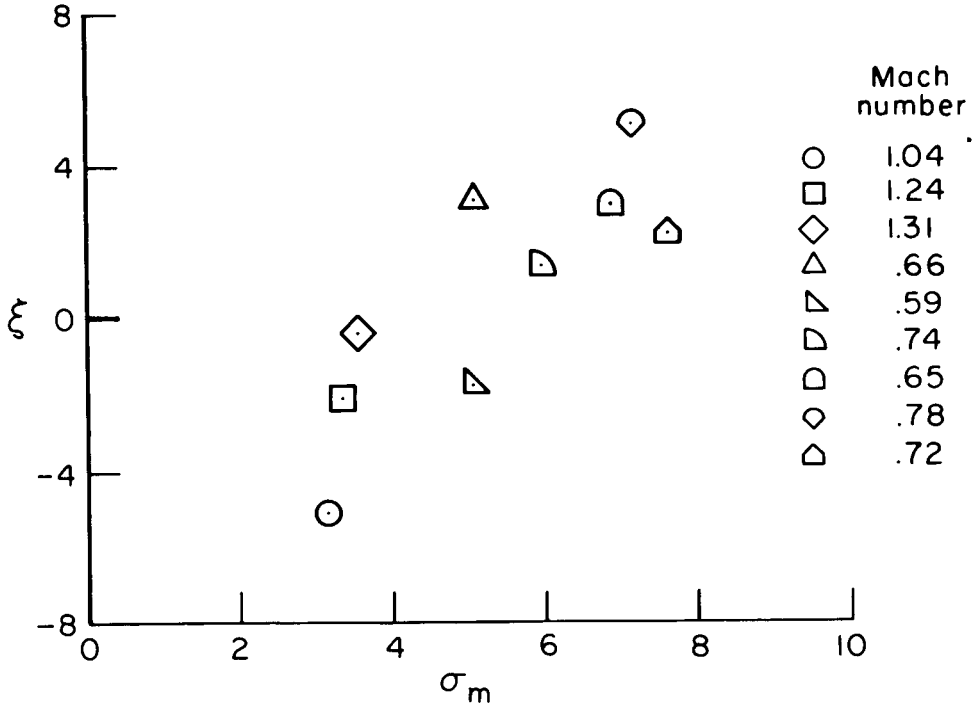


(a) Variation of dynamic-stability parameter with $\sigma_m$.

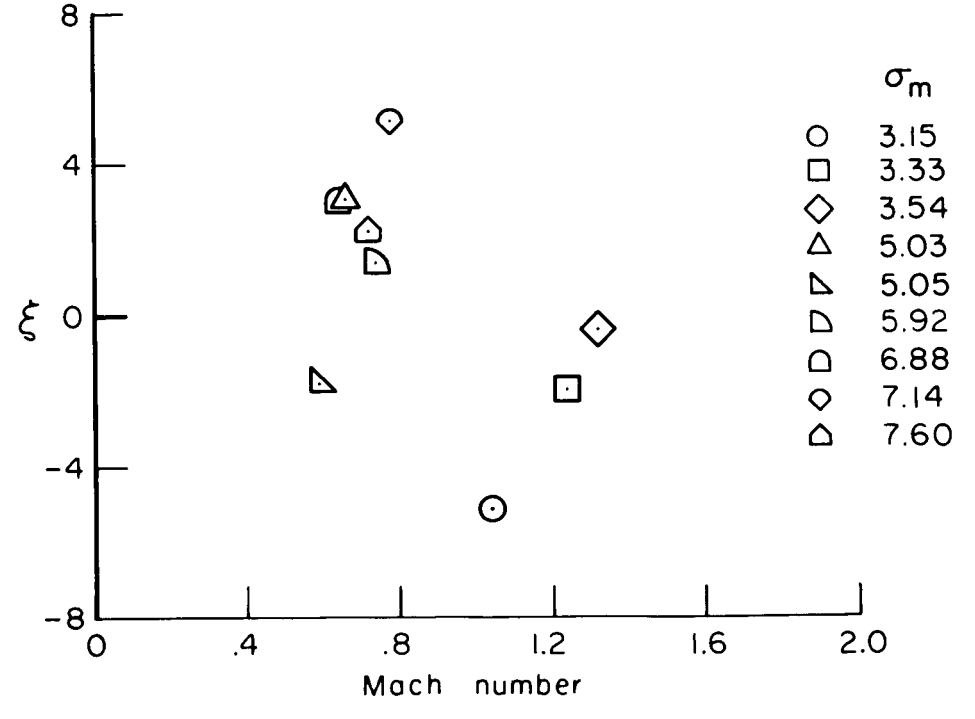


(b) Variation of dynamic-stability parameter with Mach number.

Figure 8.- Dynamic stability.

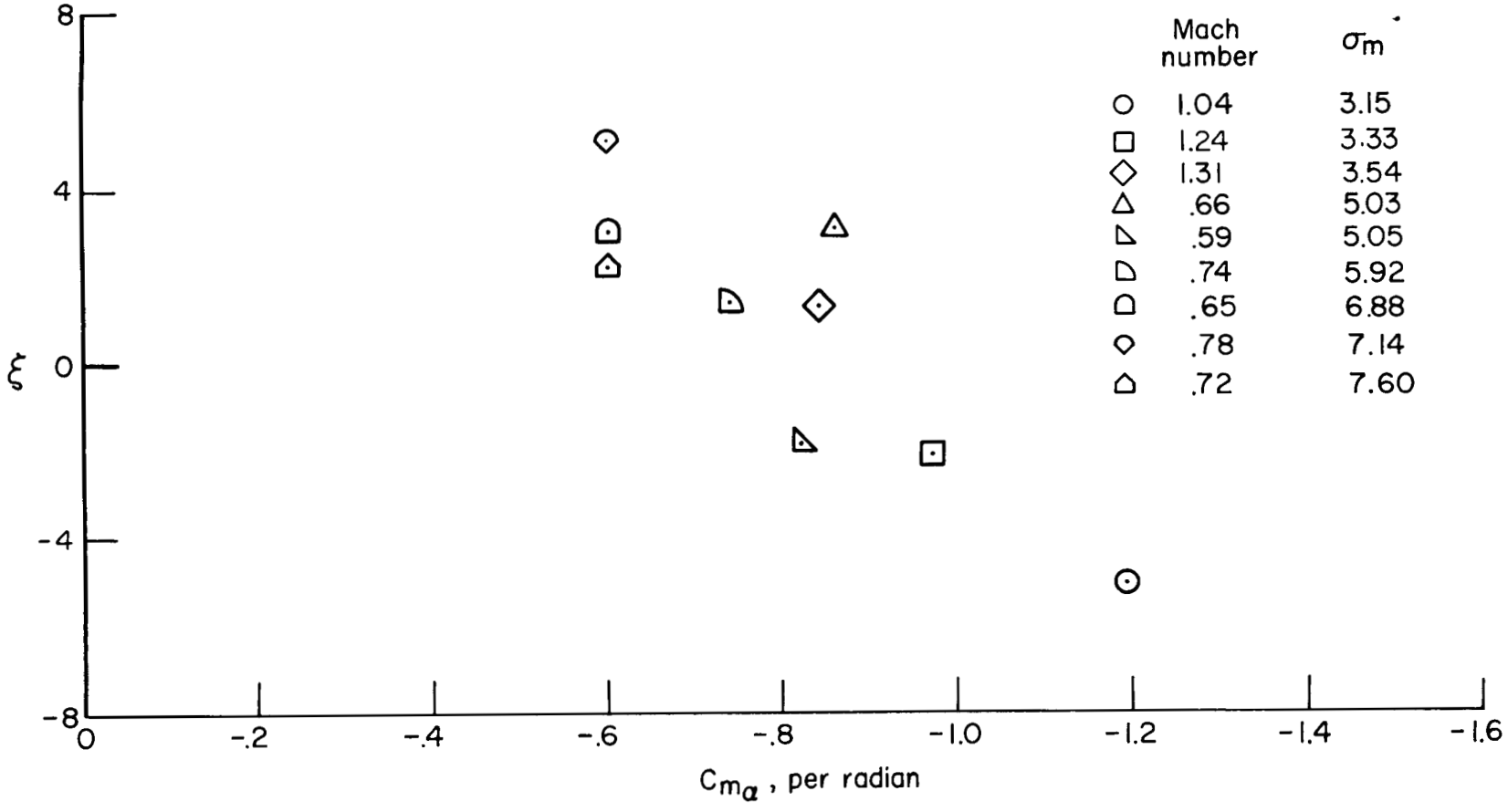


Figure 9.- Variation of dynamic-stability parameter with static-stability parameter.

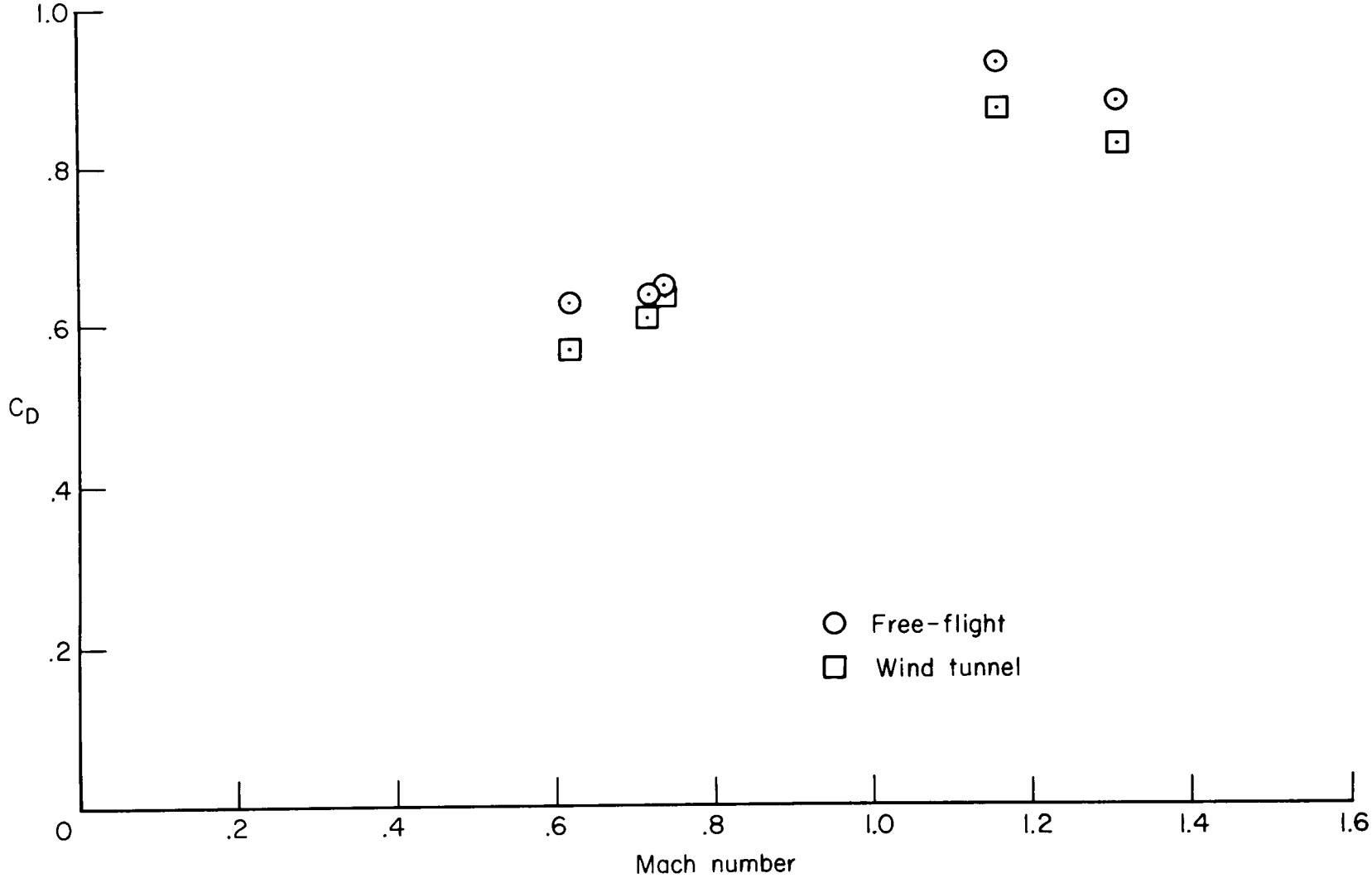


Figure 10.- Variation of drag coefficient with Mach number.

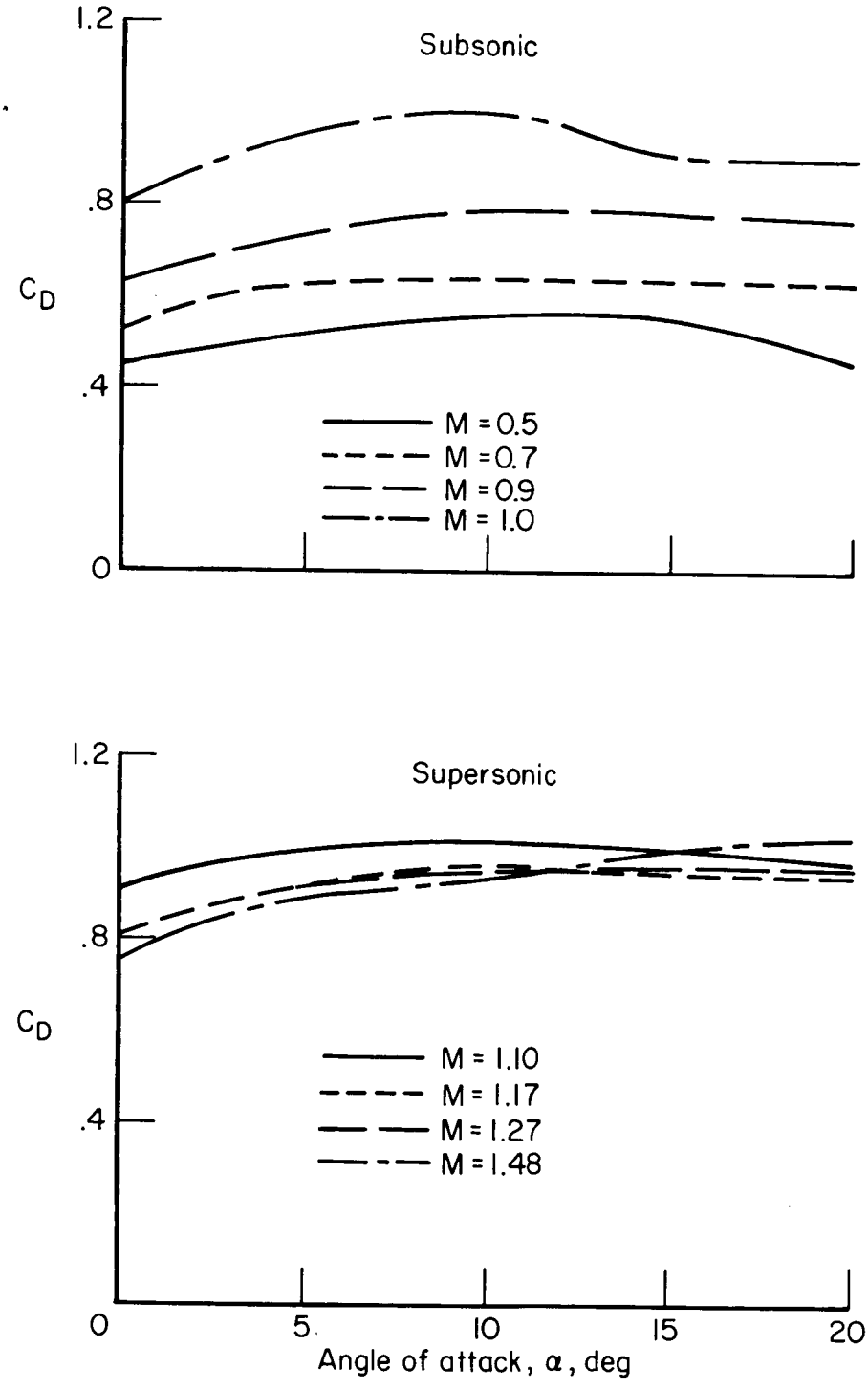


Figure 11.- Drag coefficient from wind-tunnel axial- and normal-force data.